Pixel-Level Projection of $PM_{2.5}$ Using Landsat Images and Cellular Automata Models in the Yangtze River Delta, China

Panli Tang, Yongjiu Feng, Xiaohua Tong, *Senior Member, IEEE*, Mengrong Xi, Pengshuo Li, Shurui Chen, Rong Wang, Xiong Xu, *Member, IEEE*, Chao Wang, and Peng Chen

***Abstract*—In this study, we proposed a pixel-level projection method for fine particulate matter ($PM_{2.5}$) over a long term and across a large area using a combination of Landsat images, $PM_{2.5}$ data from monitoring stations, and historical gridded $PM_{2.5}$ data. We considered the spatial dependence effects of the particulate matter using a spatial lag model to quantify the relationship between $PM_{2.5}$ concentration and land coverage indices, where the latter were calculated by the built-up, vegetation, and water indices. The future land coverage indices for the pixel-level projection of $PM_{2.5}$ were derived from the future land-use scenario predicted by the Futureland model. We applied the method to analyze the spatial patterns of $PM_{2.5}$ in the Yangtze River Delta (YRD), China, from 2000 to 2020, and then projected its pixel-level scenario in 2030. The projected $PM_{2.5}$ shows high concentrations in the north and low in the south and temporally decreases compared to 2010. The projection of the fine-grained $PM_{2.5}$ scenario can help adjust YRDs environmental and industrial policies, as well as implement its management strategies for sustainable urban development. Our method can be used to predict future patterns not only for long-term and large-scale pixel-level $PM_{2.5}$ concentrations but also for other environmental parameters.**

***Index Terms*—Cellular automata (CA), fine particulate matter ($PM_{2.5}$), land-use change, pixel-level projection, spatial lag model (SLM), Yangtze River Delta (YRD).**

I. Introduction

RAPID economic growth and industrial development have caused drastic land-use changes and reduced air quality, especially in developing countries. Among many air pollutants, fine particulate matter with a dynamic diameter of smaller than 2.5 μm ($PM_{2.5}$) has been recognized as one of the main sources [1]. The large amount of $PM_{2.5}$ emitted by human economic and social activities affects the ecological environment and is harmful to human health; for example, severe hazy weather caused by $PM_{2.5}$ may lead to frequent traffic accidents [2], and long-term exposure to high $PM_{2.5}$ can cause a variety of diseases [3], [4]. Therefore, $PM_{2.5}$ pattern analysis and scenario projection have become the major concerns of academics and environmental managers worldwide [5], [6]. The prediction of $PM_{2.5}$ is usually done at the regional level, but it is more important to perform pixel-level analysis and prediction of future scenarios.

The topics of $PM_{2.5}$ distribution in large-scale areas mainly include remote-sensing-based estimation, spatial modeling and analysis, and future scenario prediction [7], [8]. Large-scale $PM_{2.5}$ distribution estimation using remote sensing is usually performed from MODIS images and their aerosol optical depth (AOD) products, simultaneously considering the $PM_{2.5}$ truth data from ground monitoring stations as benchmarks [9]. The estimation also needs meteorological monitoring data from weather stations and remotely sensed images from satellites to examine the $PM_{2.5}$ transport [10]. With these data, the $PM_{2.5}$ estimation has been performed at the hourly, daily, weekly, monthly, and annual scales [11], [12].

The spatial modeling and analysis of $PM_{2.5}$ typically include pixel-level mapping with spatial interpolation and investigation of spatial patterns [13], [14]. Pixel-level mapping of $PM_{2.5}$ using ground monitoring station data requires the selection of a suitable spatial interpolation method, and a case study in Washington State shows that the geographical long short-term memory method can accurately interpolate the spatial pattern [15]. Based on the produced maps, scientists have found spatial dependence of $PM_{2.5}$ in most regions, which has been well confirmed by recent studies in the Yangtze River Delta (YRD) and Beijing–Tianjin–Hebei urban agglomeration of China [16], [17], [18].

Future scenario prediction of $PM_{2.5}$ is usually performed by quantitative or spatial methods, but both require a deep understanding of $PM_{2.5}$ influencing factors and their dynamic mechanisms. The principal factors influencing the distribution and diffusion can be categorized into two types: pollution

Manuscript received 18 March 2023; revised 11 June 2023; accepted 29 June 2023. Date of publication 14 July 2023; date of current version 26 July 2023. This work was supported in part by the National Key R&D Program of China under Grant 2021YFB3900105-2 and in part by the National Natural Science Foundation of China under Grant 42071371. *(Corresponding author: Yongjiu Feng.)*

Panli Tang, Yongjiu Feng, Xiaohua Tong, Mengrong Xi, Pengshuo Li, Shurui Chen, Xiong Xu, Chao Wang, and Peng Chen are with the College of Surveying and Geo-Informatics, Tongji University, Shanghai 200092, China, and also with the Shanghai Key Laboratory of Space Mapping and Remote Sensing for Planetary Exploration, Tongji University, Shanghai 200092, China (e-mail: 2210938@tongji.edu.cn; yjfeng@tongji.edu.cn; xhtong@tongji.edu.cn; ximengrong@tongji.edu.cn; lipengshuo@tongji.edu.cn; 2110969@tongji.edu.cn; xvxiong@tongji.edu.cn; wangchao2019@tongji.edu.cn; chenpeng@tongji.edu.cn).

Rong Wang is with the College of Surveying and Geo-Informatics, Tongji University, Shanghai 200092, China, and also with the Shanghai Research Institute for Intelligent Autonomous Systems, Tongji University, Shanghai 200092, China (e-mail: 2210960@tongji.edu.cn).

Digital Object Identifier 10.1109/JSTARS.2023.3294614

sources and meteorological conditions, both are closely related to land-use status in spatial terms [19]. Specifically, land-use type, landscape configuration, and urban patterns are typical land cover factors that influence $PM_{2.5}$ distribution [20]. Based on the recognition of the formation and diffusion of $PM_{2.5}$, some scientists have used numerical simulations or quantitative methods to implement predictions of future scenarios. For example, several methods, including random forest, deep learning, and nonlinear seasonal gray models, have been applied to quantitatively predict short-term (e.g., half-day, one day, and three days) $PM_{2.5}$ [21], [22], [23]. In contrast, pixel-level future scenario predictions may be more valuable, but existing studies have focused more on short-time (weekly, monthly, and annual) future predictions. For example, modelers utilized the random forest and geographically and temporally weighted regression (GTWR) methods to derive daily and annual pixel-level predictions of $PM_{2.5}$ at the 1 km spatial resolution [24], [25].

Despite the current progress in methods and case studies on $PM_{2.5}$ projections, the effects of land use and land coverage and the spatial dependence of $PM_{2.5}$ have not been considered sufficiently, thus posing limitations to our ability in performing long-term and large-scale future scenario predictions. Therefore, two essential questions are yet to be addressed: First, how to establish the relationship between $PM_{2.5}$ and land coverage accurately by considering the spatial dependence effects of $PM_{2.5}$?; second, how to project the pixel-level long-term $PM_{2.5}$ distribution by predicting future land-use scenarios? The answers to these questions can fill the gaps in our knowledge of the long-term changes in $PM_{2.5}$ at the pixel level, aiming to provide reliable spatial data for improving air environmental quality and enhancing regional sustainable development.

The purpose of this study is to develop a new method for predicting future $PM_{2.5}$ distributions at the pixel level over the long term (e.g., ten years) and large scale. We assumed that since the land-use pattern is proven to be related to $PM_{2.5}$, we can establish the relationship between land coverage indices and the $PM_{2.5}$ concentrations considering the spatial dependence. The future indices, such as normalized difference built-up index (NDBI), normalized difference vegetation index (NDVI), and normalized difference water index (NDWI), can be calculated using the land-use patterns. In addition, the prediction of the land-use scenario by cellular automata (CA) based approach is practical, thus allowing us to predict future $PM_{2.5}$ scenarios based on the future land-use scenario. In this study, we developed a method for $PM_{2.5}$ projection based on the above assumptions and validated the method in the YRD of China by predicting its $PM_{2.5}$ scenario in 2030. The proposed method of $PM_{2.5}$ projection can help authorities to make sound decisions on air pollution control.

II. Methodology

A. Study Area

The YRD region (29°20′N-32°34′N, 115°46′E-123°25′E) is located at the lower reaches of the Yangtze River in eastern China and is the most economically developed area in the country. This region consists of Shanghai, Jiangsu, Zhejiang, and Anhui provinces, covering 26 cities [see Fig. 1(a)] with a total area of 211 700 km^2. YRD has a subtropical monsoon climate with hot rainy summers and cold dry winters, and the elevation is low in the northeast and high in the southwest. The region has a resident population of ∼165 million, a gross domestic product (GDP) of ∼20.5 trillion RMB, and an average urbanization rate of ∼75% in terms of the proportion of urban residents. YRD contributes ∼20% of the country's GDP with only 2.2% of the land area and 11.7% of the population.

It is noted that rapid urbanization and industrialization may lead to negative effects on the environment, especially land-use change and severe air pollution, where $PM_{2.5}$ is an important indicator of air quality. By 2020, there were 165 ground monitoring stations of $PM_{2.5}$ in YRD [see Fig. 1(b)]. As an important intersection between the "Belt and Road" and the Yangtze River Economic Belt, YRD plays a crucial role in the sustainable development of the belt and even around the world [26]. Therefore, it is of great theoretical and practical value to study the spatial patterns and future scenarios of $PM_{2.5}$ for building a sustainable YRD.

B. Raw Datasets

We used Landsat-5 TM and Landsat-8 OLI images (earthexplorer.usgs.gov) to produce land-use patterns and land coverage indices. We also collected ground monitoring station $PM_{2.5}$ (cnemc.cn) to explore its relationship with the land coverage indices and applied historical gridded $PM_{2.5}$ data in 2010 (sites.wustl.edu) to validate the method. To predict land-use scenarios based on their influencing factors, we collected socioeconomic and topographical data, including population density, GDP, digital elevation model (DEM), points of interest (POIs), transport, and river networks [27] (see Table I). Among these, the population density maps were accessed from Worldpop (hub.worldpop.org), the GDP maps were produced by Kummu et al. [28], the DEM maps were collected from ASTER GDEM 2 (gscloud.cn), and the POIs were extracted from OpenStreetMap (openstreetmap.org). All factors were converted to gridded data with a spatial resolution of 100 m, facilitating the subsequent modeling and mapping of $PM_{2.5}$. Among these, we downscaled the GDP product from 1000 to 100 m, but this did not improve the quality of this dataset; thus, these downscaled data are equivalent to the original but allowed for a uniform resolution in the modeling.

C. Methods

For spatial analysis and future scenario prediction of $PM_{2.5}$, we developed a new method that considers the future land-use change prediction and the spatial dependence effects of $PM_{2.5}$ (see Fig. 2). The method includes three parts: land-use projection, land coverage indices projection, and $PM_{2.5}$ projection. First, the land-use projection was performed using the Futureland model, a state-of-the-art software that is applicable to multiple land-use change simulations with paralleled computation [29]. Second, since the land coverage indices are closely related to the land-use and $PM_{2.5}$ patterns, the structural–local variations method (SLVM) was used to predict the land coverage

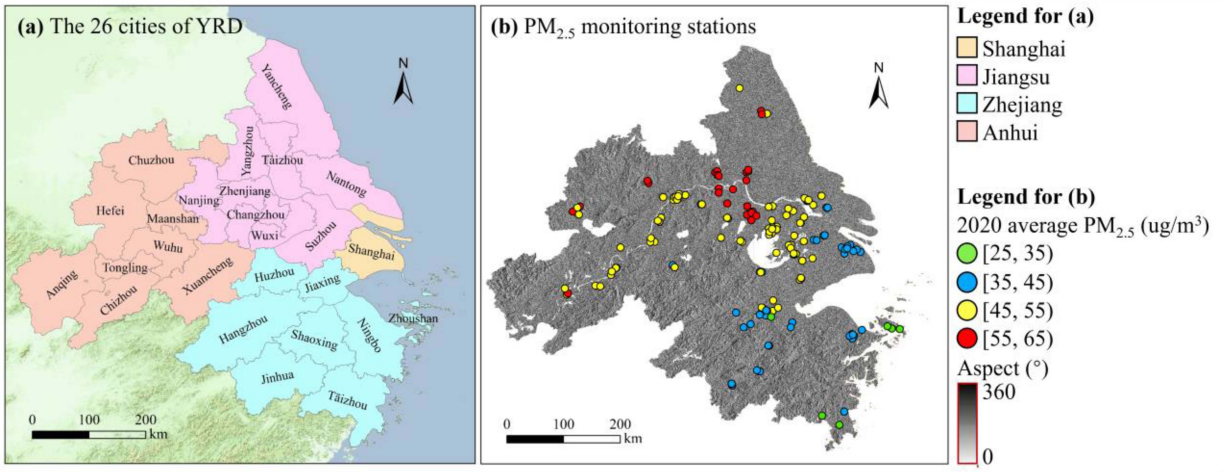

Fig. 1. (a) YRD study area with 26 cities. (b) Ground monitoring stations of $PM_{2.5}$ concentrations.

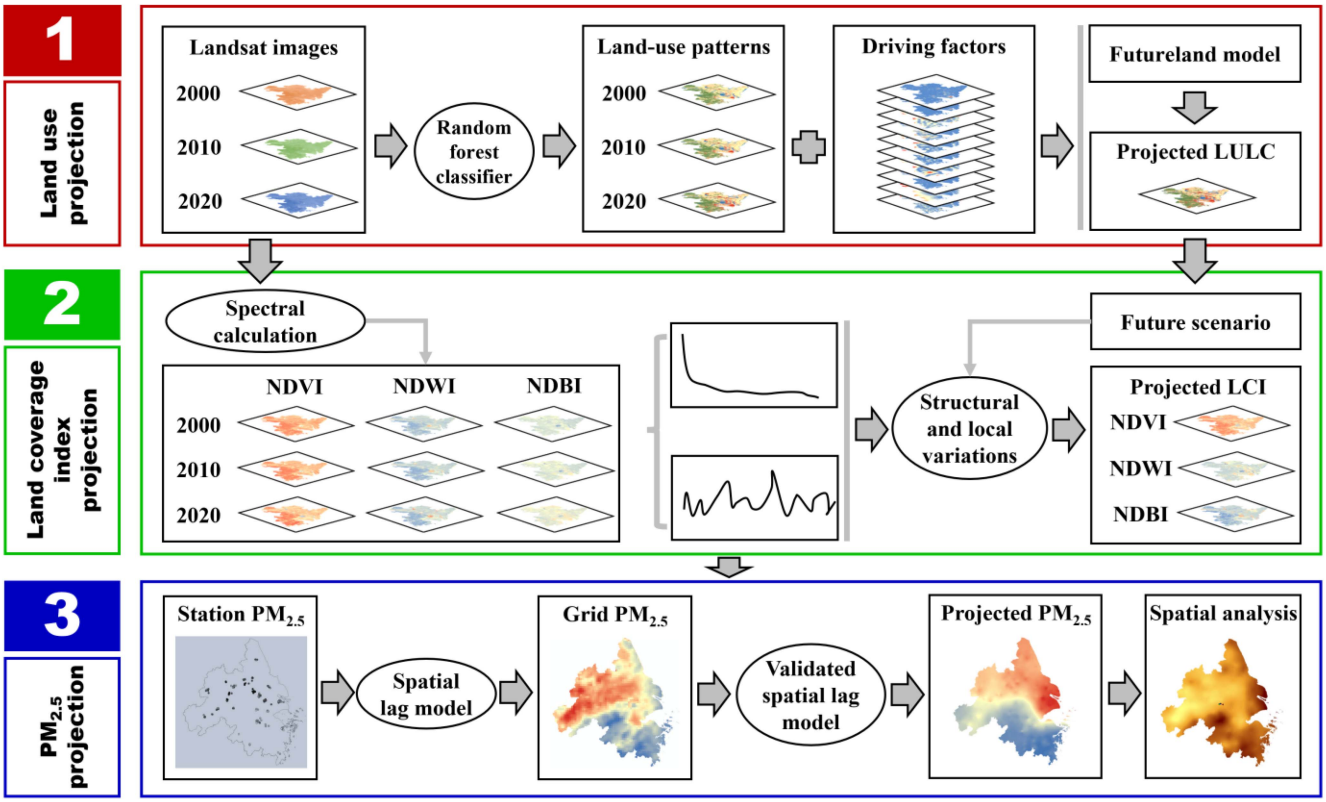

Fig. 2. Workflow of pixel-level projection of $PM_{2.5}$ using Futureland and SLM.

indices. Third, considering the future land-use change and the spatial dependence of $PM_{2.5}$, we predicted the future $PM_{2.5}$ pattern based on the spatial lag model (SLM) and conducted the spatial analysis consequently.

1) Futureland-Based Land-Use Projection Model: Land-use projection models are commonly built considering the relationship between past land-use change and its driving factors, where the past and present land-use patterns are often produced using remote-sensing images and classifiers. In this study, we utilized the random forest classifier to produce the land-use pattern in 2000, 2010, and 2020 using the Landsat images by following the article presented by Orieschnig et al. [30] since this classifier has high accuracy and strong ability of multidimensional data handling. Before the image classification, we defined land-use categories as four types, including built-up, agricultural, forest, and water (see Table II), according to the criteria suggested by the Ministry of Natural Resources of China (globallandcover.com) and European Space Agency (due.esrin.esa).

TABLE I
REMOTE-SENSING IMAGES, PRODUCTS, AND VECTOR DATASETS USED IN THIS STUDY

Type	Name	Source	Date	Spatial resolution	Purpose
Remote sensing images	Landsat-5 TM	United States Geological Survey	2000, 2010	30m	Produce land-use pattern and land coverage indices in 2000 and 2010
	Landsat-8 OLI	United States Geological Survey	2020	30m	Produce land-use pattern and land coverage indices in 2020
Monitoring data	$PM_{2.5}$ (Ground monitoring stations)	China National Environmental Monitoring Centre	2020		Build the relationship between $PM_{2.5}$ and land coverage indices
	Gridded $PM_{2.5}$	Washington University	2010	1000m	Assess the modeling results
Remote sensing products	Population density	WorldPop	2020	100m	Produce the population density factor
	GDP	nature.com/articles/sdata20184	2015	1000m	Produce the economic factor
	DEM	Geospatial Data Cloud	2015	30m	Produce the terrain factor
Vector data	City centers	OpenStreetMap	2020		Produce the proximity to city centers
	Town centers	OpenStreetMap	2020		Produce the proximity to town centers
	Highways	OpenStreetMap	2020		Produce the proximity to highways
	Primary roads	OpenStreetMap	2020		Produce the proximity to primary roads
	Railways	OpenStreetMap	2020		Produce the proximity to railways
	Subways	OpenStreetMap	2020		Produce the proximity to subways
	Rivers	OpenStreetMap	2020		Produce the proximity to rivers

TABLE II
DEFINITION OF LAND-USE CATEGORIES AND THEIR IMAGE FEATURES IN YRD

Land-use classification	Definition	Geometric features	Spectral features
Built-up	Land for impermeable surface areas	Regular or irregular block geometry	Reflected by near-infrared and shortwave infrared bands
Agricultural	Land for crops, horticulture, garden, grass and shrub	Planar, striated or block geometries with relatively homogeneous texture	Reflected by green and red bands
Forest	Land covered by forests	Irregular geometry influenced by topography, with a single texture	Reflected by near-infrared and red bands
Water	Land covered by water bodies	Striated or dendritic geometry	Reflected by green and near-infrared bands

In this study, the CA-based Futureland model was applied to simulate and project the future land-use pattern. CA defines the state of a land cell at present as a function of the state of the land cell itself and the effect of its neighboring cells at the previous time by a set of transition rules [31], [32]. Generalized logistic regression (GLR) is applied in the Futureland to construct the relationship between the driving factors and land-use types [33]. The Futureland model has three advantages:

1) applying different driving factors for different land-use types in a single simulation scenario;
2) projecting land-use demand using the Markov chain and considering local constraints;
3) using data blocking-based parallel computing to optimize and accelerate the simulation process.

The Futureland model consists of five core elements, including land cell, probability-of-occurrence (POO), neighborhood effect, conversion cost, and local and global constraints. The total transition rules of Futureland can be given by [34]

$$P(S_i^{t+1}) = \mathrm{POO}_{\mathrm{con}} \times P_{n(h,u)} \times (1 - \mathrm{Cost}_{c\to p}) \times (1 - \mathrm{Res}) \tag{1}$$

where $P(S_i^{t+1})$ is the total transition probability for a land cell i to change its state; $\mathrm{POO}_{\mathrm{con}}$ is the POO defined by driving factors; $P_{n(h,u)}$ is the neighborhood effect; $\mathrm{Cost}_{c\to p}$ is the conversion cost; and Res is the constraint.

The POO reflects the possibility of each land-use type converting its state, and this probability is a crucial part of the transition rules. In the Futureland model, GLR is utilized to derive the POO because different land-use types are influenced by the same or different factors. The GLR-based POO can be given by

$$\mathrm{POO}_{\mathrm{con},r} = \left(\frac{e^{\beta_0 + \sum_{i=0}^{n} \lambda_i \beta_i X_i}}{1 + e^{\beta_0 + \sum_{i=0}^{n} \lambda_i \beta_i X_i}} \right)_r \tag{2}$$

where $\mathrm{POO}_{\mathrm{con},r}$ is the POO of land-use type r; n is the total number of driving factors; X_i is the ith driving factor; β_0 is a constant; β_i is the regression coefficient of factor X_i; and λ_i is introduced to indicate the presence or absence of a certain factor, with 1 being present and 0 being excluded.

The neighborhood effect can be defined by the neighborhood configurations and weights that represent the ability of each neighbor to influence the central cell. For land-use type u, the neighborhood effect on the central cell h can be given by [35]

$$P_{n(h,\,u)} = \left(\frac{\sum_{k=1}^{N\times N-1} \mathrm{con}(w_{k\to u})}{N\times N-1} \right)_h \tag{3}$$

where $N \times N$ is the neighborhood size with a square configuration; and $\mathrm{con}(w_{k\to u})$ is the effect of the neighbor k on the central cell h when converting to land-use type u.

The conversion cost is one of the important components of land-use change and represents the socioeconomic costs of changing from one land-use type to another. In the Futureland model, the conversion cost from one land-use type to another can be defined by the modelers according to the theoretical analysis. To project the future land demand for each type, we used a modified Markov chain method to compute the total amount of land as a global constraint [36]. Markov chain is a stochastic process in which time and state are discrete, which predicts the future state of a random variable based on a transition probability matrix. The future land demand can be given by [37]

$$L_{\mathrm{DEMAND}}^{t+1} = L_{\mathrm{DEMAND}}^{t} \times \begin{bmatrix} P_{11} & \cdots & P_{1m} \\ \vdots & P_{qr} & \vdots \\ P_{m1} & \cdots & P_{mm} \end{bmatrix} \times \alpha \tag{4}$$

where L_{DEMAND}^{t} and $L_{\mathrm{DEMAND}}^{t+1}$ are the land quantities at time t and time $t+1$, respectively; m is the total number of land-use types; P_{qr} is the land transformation probability from land-use type q to land-use type r, determined by the percentage of area converted from q to r ($0 \le P_{qr} \le 1$); $\sum_{r=1}^{m} P_{qr} = 1$; and α is a predefined adjust coefficient of the Markov chain for urban expansion.

2) SLVM-Based Land Coverage Indices Projection Model: In this study, we derived three land coverage indices (NDBI, NDVI, and NDWI) by spectral calculation. Among these, NDBI indicates the density of built-up [38], NDVI indicates the vegetation distribution and density [39], and NDWI indicates the density of water bodies and water-bearing soil [40]. When using Landsat TM or OLI images, three indices can be calculated by [41]

$$\begin{cases} \mathrm{NDBI} = \frac{\mathrm{MIR}-\mathrm{NIR}}{\mathrm{MIR}+\mathrm{NIR}} = \frac{B5-B4}{B5+B4}\ (\mathrm{TM}) = \frac{B6-B5}{B6+B5}\ (\mathrm{OLI}) \\ \mathrm{NDVI} = \frac{\mathrm{NIR}-\mathrm{Red}}{\mathrm{NIR}+\mathrm{Red}} = \frac{B4-B3}{B4+B3}\ (\mathrm{TM}) = \frac{B5-B4}{B5+B4}\ (\mathrm{OLI}) \\ \mathrm{NDWI} = \frac{\mathrm{GREEN}-\mathrm{NIR}}{\mathrm{GREEN}-\mathrm{NIR}} = \frac{B2-B4}{B2+B4}\ (\mathrm{TM}) = \frac{B3-B5}{B3+B5}\ (\mathrm{OLI}) \end{cases} \tag{5}$$

where MIR is the shortwave infrared band; NIR is the near-infrared band; RED is the red band; and GREEN is the green band.

Based on the calculated historical land coverage indices, we applied the SLVM to project future indices considering their structural and local variations that reflect the spatiotemporal evolution [42]. This method was initially proposed by Feng et al. [42] in predicting the spatial variation of land surface temperature and urban heat islands, which was validated in the Taihu Lake basin of China. The structural variations are characterized by temporal evolution, which is related to the change in land coverage indices over time. However, the local variations are characterized by the spatial evolution associated with the land-use change and pattern.

3) SLM-Based $PM_{2.5}$ Projection Model: SLM is a global spatial regression model that uses spatially weighted neighbors as spatial lags and uses them as a key independent variable. The method is a typical spatial autoregressive model that can be used to handle variables with strong spatial dependence [43]. Considering that the $\mathrm{PM}_{2.5}$ distribution is of spatial dependence, we adopted SLM to simulate and predict the spatial pattern of $\mathrm{PM}_{2.5}$. SLM can be given by [44]

$$\boldsymbol{Y} = \rho \boldsymbol{W} \boldsymbol{Y} + \beta_1 \boldsymbol{X}_1 + \beta_2 \boldsymbol{X}_2 + \beta_3 \boldsymbol{X}_3 + \varepsilon \tag{6}$$

where $\boldsymbol{Y}$ is an $N\times 1$-dimensional vector of the dependent variable ($\mathrm{PM}_{2.5}$); ρ is the coefficient of the spatial lag, measuring the magnitude of spatial dependence; $\boldsymbol{W}$ is the spatial weight matrix, defining the distance-influenced neighbor relationships; $\boldsymbol{X}_1$, $\boldsymbol{X}_2$, and $\boldsymbol{X}_3$ are the $N\times 1$-dimensional vector of the explanatory

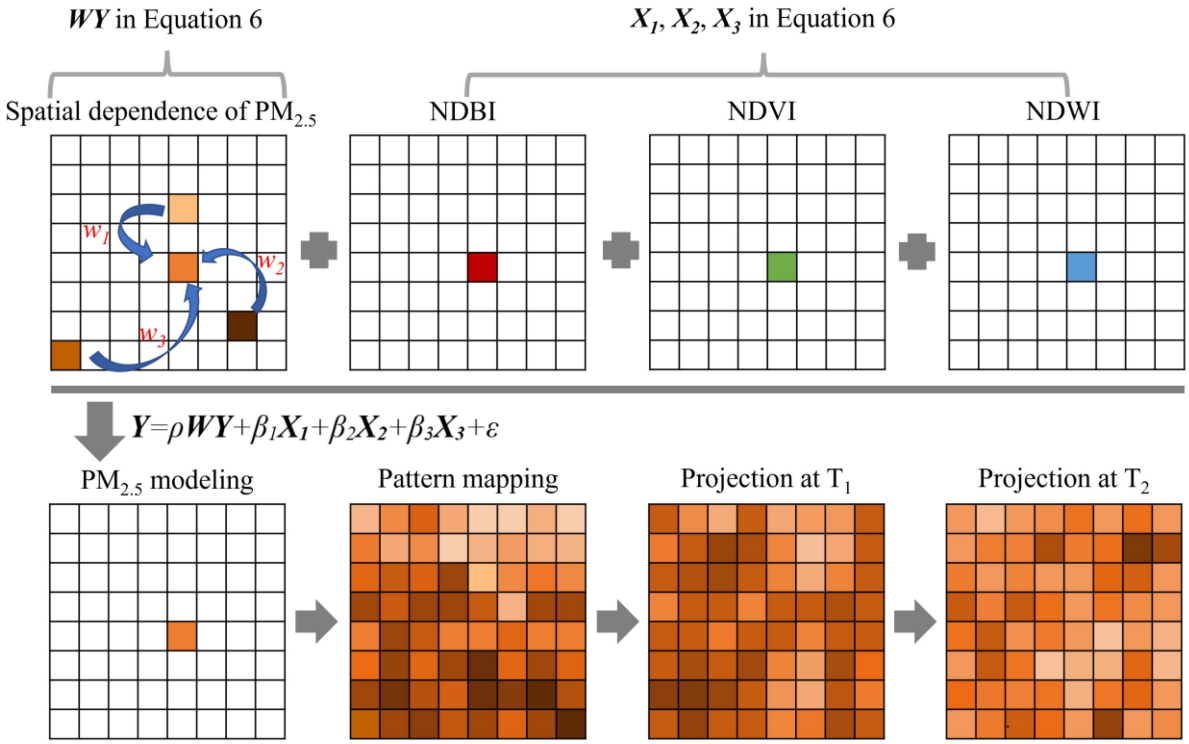

Fig. 3. SLM-based modeling and projection of $PM_{2.5}$ based on spatial dependence, NDBI, NDVI, and NDWI.

variables (NDBI, NDVI, and NDWI, respectively); β_1, β_2, and β_3 are the coefficients of the explanatory variables, successively; and ε is the random error.

Fig. 3 shows the $PM_{2.5}$ modeling at a specific pixel as an example based on the spatial dependence of $PM_{2.5}$ and the influencing factors, such as NDBI, NDVI, and NDWI. When the $PM_{2.5}$ of each pixel is linked reliably with the independent variable, a modeling equation is derived to produce the $PM_{2.5}$ map. Furthermore, by considering the predicted future land coverage indices, we predicted the future pixel-level $PM_{2.5}$ using (6).

D. Validation Methods

1) Cell-by-Cell Overall Fuzzy Accuracy (OFA): We proposed the OFA to evaluate the $PM_{2.5}$ modeling results. This method describes the overall accuracy of comparing the modeled raster map with the reference raster map, which is similar to the evaluation of land-use classification [45]. The difference between OFA and overall accuracy is that pixels in the former are measured in terms of continuous values rather than types. Therefore, for modeled or predicted $PM_{2.5}$ of a specific pixel, the modeling method is considered accurate if the difference is within a predefined threshold (δ) compared with the pixel value in the reference map. The OFA can be given by

$$\begin{cases} \mathrm{OFA} = \frac{T}{T+F} \\ T,\ \delta = \frac{\mathrm{PM}_{2.5m}-\mathrm{PM}_{2.5r}}{PM_{2.5r}} \le 10\% \\ F,\ \delta = \frac{\mathrm{PM}_{2.5m}-\mathrm{PM}_{2.5r}}{\mathrm{PM}_{2.5r}} > 10\% \end{cases} \tag{7}$$

where T and F are the total numbers of correctly and incorrectly simulated pixels, respectively; the threshold (δ) is the relative error; $\mathrm{PM}_{2.5m}$ and $\mathrm{PM}_{2.5r}$ are the modeled and reference $PM_{2.5}$, respectively. In this study, we define the δ as smaller than 10%, which indicates that the results are considered correct if the difference between the modeled and reference results is smaller than such threshold.

2) Random Point-Based Accuracy: Apart from cell-by-cell OFA evaluation, we also assessed the random points selected from the modeled $PM_{2.5}$ map and compared them with the reference map from the article presented in [46]. This is a cross validation of the model, which assesses how well the sample points match between the modeled and reference map. We applied the correlation coefficient (R^2) to indicate the fitting performance and the root-mean-square error (RMSE) to estimate the residual distribution. The R^2 and RMSE can be given by

$$\begin{cases} R^2 = \sqrt{\frac{\sum_{i=1}^{n}\left(\mathrm{PM}_{2.5mi}-\overline{\mathrm{PM}_{2.5r}}\right)^2}{n\sum_{i=1}^{n}\left(\mathrm{PM}_{2.5ri}-\overline{\mathrm{PM}_{2.5r}}\right)^2}} \\ \mathrm{RMSE} = \sqrt{\frac{\sum_{i=1}^{n}\left(\mathrm{PM}_{2.5mi}-\mathrm{PM}_{2.5ri}\right)^2}{n}} \end{cases} \tag{8}$$

where n is the total number of sample points; i is the ith sample point; $\mathrm{PM}_{2.5mi}$ and $\mathrm{PM}_{2.5ri}$ are the modeled and reference $PM_{2.5}$ of the ith sample, respectively; and $\overline{\mathrm{PM}_{2.5r}}$ is the average of the reference $PM_{2.5}$. A higher R^2 indicates a better fitting and a smaller RMSE indicates a higher accuracy.

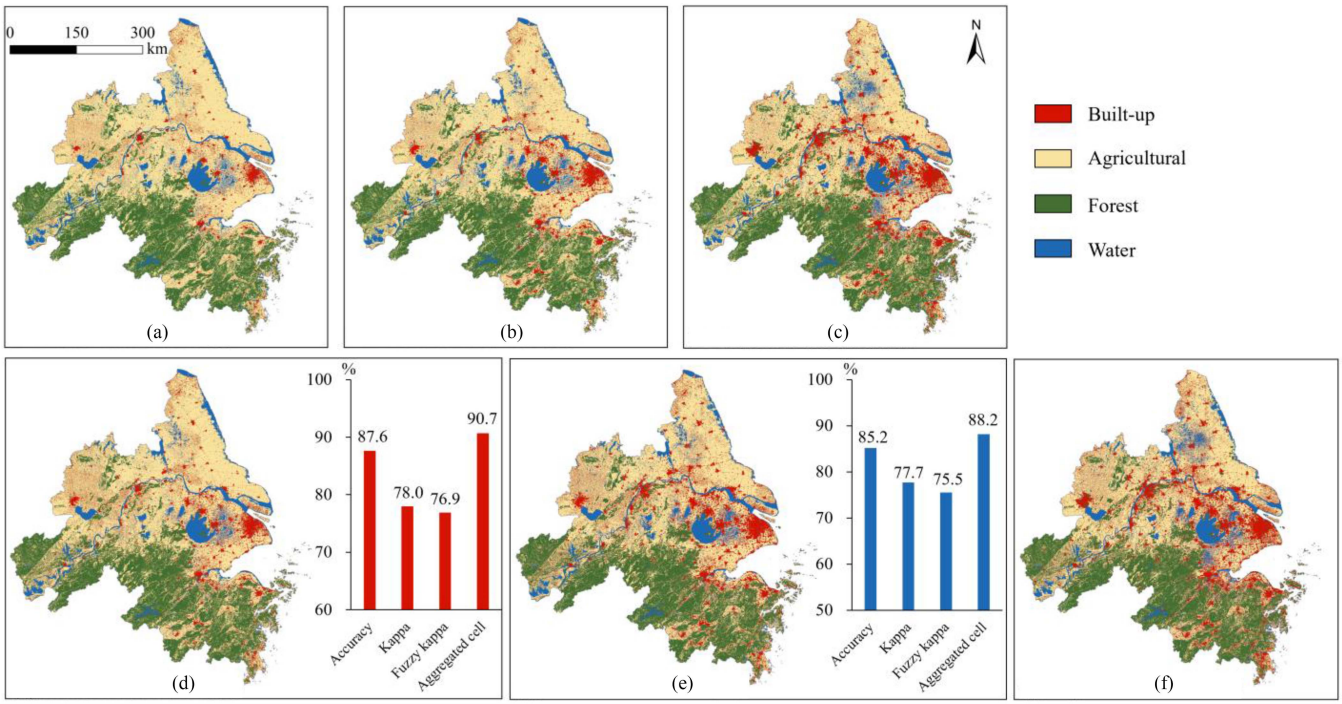

Fig. 4. Observed, simulated, and projected land-use patterns 2000–2030 in YRD. (a) Observed land use 2000. (b) Observed land use 2010. (c) Observed land use 2020. (d) Simulated land use 2010. (e) Simulated land use 2020. (f) Projected land use 2030.

TABLE III
OBSERVED AND PREDICTED LAND-USE CHANGE 2000–2030 IN YRD

Year/Period	Land-use type (%)				
	Built-up	Agricultural	Forest	Water	Total
2000	6.0	56.1	29.0	8.9	100.0
2010	8.8	53.5	28.9	8.8	100.0
2020	13.5	48.0	28.9	9.6	100.0
2030	17.1	44.0	28.7	10.2	100.0
2000-2010	2.8	-2.7	-0.1	-0.1	
2010-2020	4.7	-5.5	-0.1	0.9	
2020-2030	3.6	-4.0	-0.2	0.6	

III. RESULTS

A. Projection of Land-Use Pattern

Fig. 4(a)–(c) shows a significant increase in the built-up during 2000–2020, as evidenced by the land-use maps produced from Landsat images, with overall accuracy above 89% for all years. The built-up is primarily distributed along the Yangtze River and the coastal economic zone, the agricultural is largely allocated in the central and northern areas with flat terrain and fertile soil, the forest is majorly distributed in Zhejiang Province and Anhui Province of YRD, and the water is primarily the Yangtze River, various lakes in the flat areas, and coastal waters. Table III presents that during the last 20 years from 2000 to 2020, the built-up of YRD has expanded significantly while the agricultural has decreased significantly, and the areas of forest and water are relatively stable, indicating the urban encroachment on prime agricultural land.

Before the pixel-level projection using Futureland, we predicted the land-use demand in 2030 using the modified Markov chain, which indicates an increase of built-up by 3.6% and a decrease of agricultural by 4% (see Table III). Futureland was calibrated by simulating the land-use pattern in 2010 and validated by simulating the land-use pattern in 2020 [see Fig. 4(d) and (e)], with an overall accuracy of 87.6% and 85.2%, respectively. This indicates that the constructed Futureland model is effective, and therefore, we applied it to project YRDs 2030 land-use

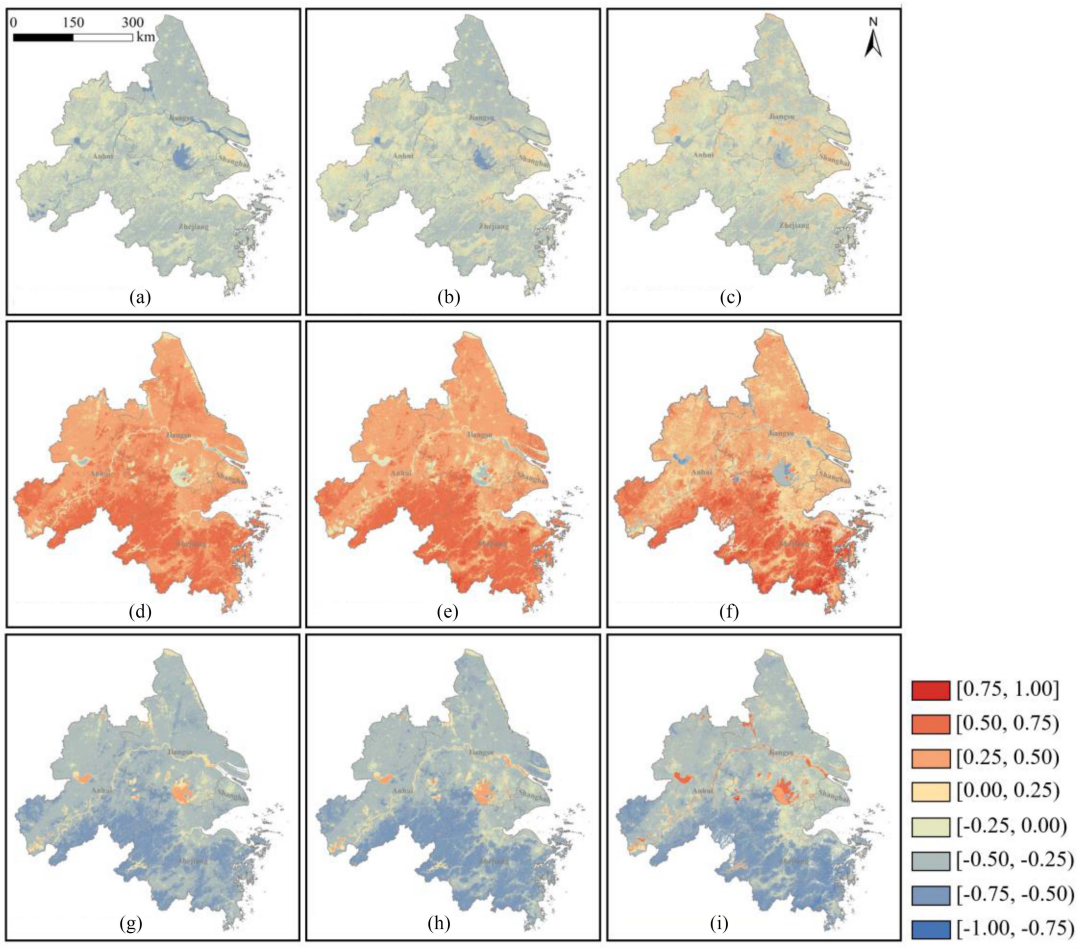

Fig. 5. Land coverage indices 2000–2020 in YRD. (a) NDBI 2000. (b) NDBI 2010. (c) NDBI 2020. (d) NDVI 2000. (e) NDVI 2010. (f) NDVI 2020. (g) NDWI 2000. (h) NDWI 2010. (i) NDWI 2020.

scenario [see Fig. 4(f)]. During 2020–2030, there are significant land-use changes in quantities and spatial patterns, especially in built-up and agricultural land. While the cities in YRD are typically distributed in flat or low-lying areas, 2030 built-up continues to expand around the existing cities, encroaching on the surrounding agricultural land to develop more distinctive living, industrial, and economic zones. Consequently, such an intense land-use change leads to significant environmental changes in the coming decade, accompanied by intensifying human activities that drive the spatiotemporal evolution of air quality.

B. Projection of Land Coverage Indices

The land coverage indices (i.e., NDBI, NDVI, and NDWI) in 2000, 2010, and 2020 were acquired for projecting those in 2030. Since all three indices have a value range of 0–1, we adopted the same color to represent the same attribute value in Fig. 5, where NDVI has the highest average, while NDWI has the lowest average. Overall, the spatial patterns of the three land coverage indices are highly similar to the land-use pattern of the respective years. For example, high NDBI is primarily found in built-up, while low NDBI is primarily found in agricultural, forest, and water areas. High NDVI primarily occurs in the forest of the southern YRD, while low NDVI mostly occurs in the northern part, and NDVI in the forest increases, while NDVI in other land-use types decreases during 2000–2020. NDWI of water is the highest, followed by built-up, agricultural, and forest, with an increasing trend during 2000–2020.

We then applied SLVM to project the three land coverage indices for 2030 (see Fig. 6) based on the 2030 land-use scenario. In terms of index domain and spatial profile, the predicted three indices of 2030 have relatively high similarity to the spatial pattern of 2000–2020, indicating the reasonability of our prediction. Similarly, NDVI shows the highest average and NDWI shows the lowest average, and their patterns are significantly influenced by the land-use pattern. There is significant spatiotemporal heterogeneity in the land coverage indices, with an increase of NDBI in built-up, an increase of NDVI in all areas except built-up, and an increase of NDWI in water areas in a few local regions. These drastic changes in land use and land coverage indices suggest that the YRDs $PM_{2.5}$ in 2030 may also change significantly.

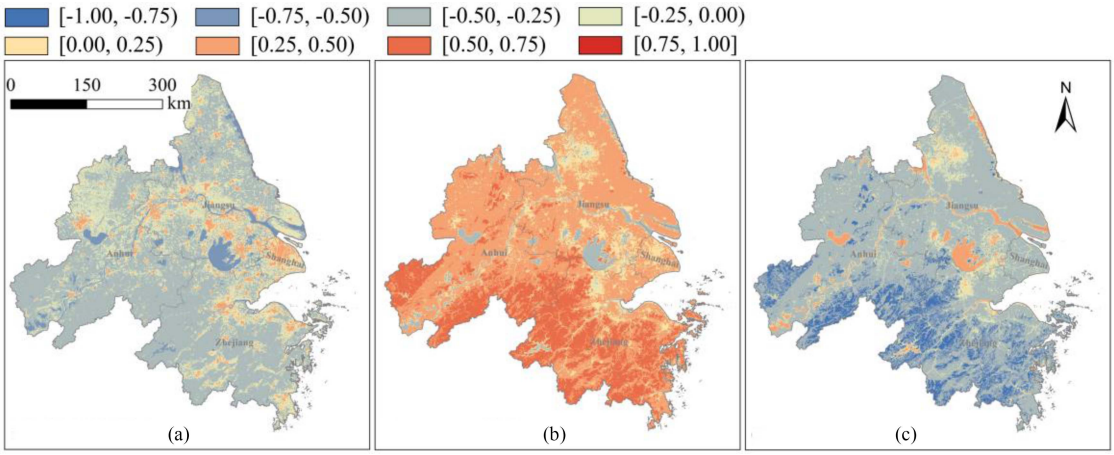

Fig. 6. Projected land coverage indices of YRD in 2030. (a) NDBI 2030. (b) NDVI 2030. (c) NDWI 2030.

C. *Projection of Pixel-Level $PM_{2.5}$ Scenario to the Year 2030*

To project the pixel-level $PM_{2.5}$ scenario in 2030, we assumed that $PM_{2.5}$ is correlated with the three land coverage indices mentioned above and the relationship varies spatially but not temporally. The construction of this relationship requires the fitting of historical $PM_{2.5}$ and land coverage indices. Through intensive testing and analysis, we used the SLM method to construct this relationship, which well explained the influence of $PM_{2.5}$'s spatial dependence and the land coverage indices on the relationship. The SLM with the specified parameters can be given by

$$\boldsymbol{PM}_{2.5} = 0.95 \times \boldsymbol{W} \times \boldsymbol{PM}_{2.5} + 2.14 \times \boldsymbol{X}_1 - 1.64 \times \boldsymbol{X}_2 - 0.44 \times \boldsymbol{X}_3 + 2.71 \quad (9)$$

where $\boldsymbol{W}$ is the spatial weight matrix; $\boldsymbol{X_1}$, $\boldsymbol{X_2}$, and $\boldsymbol{X_3}$ are the NDBI, NDVI, and NDWI, respectively. The goodness-of-fit of SLM is 0.87, showing a well-modeling performance.

The equation we acquired shows that $PM_{2.5}$ is positively correlated to its nearby $PM_{2.5}$ profile and NDBI, while it is negatively correlated to NDVI and NDWI. Among the three land coverage indices, NDBI has the strongest effect on $PM_{2.5}$ because it has the largest coefficient. We calibrated SLM using the ground monitoring station data for 2020 [see Fig. 7(a)], and then validated the model using the 2010 gridded product [see Fig. 7(c)] to yield the $PM_{2.5}$ maps for 2020 [see Fig. 7(b)] and 2010 [see Fig. 7(d)]. These maps show that the overall patterns are generally consistent for the 2020 reference $PM_{2.5}$ and modeled $PM_{2.5}$ in the model calibration, and for the 2010 reference $PM_{2.5}$ and modeled $PM_{2.5}$ in the model validation. The cell-by-cell quantitative assessment indicates a high OFA of 83.1% for calibration and 89.7% for validation. The random point-based assessment shows a high correlation (R^2) of 0.8 and a relatively low RMSE of 0.3 when validating the $PM_{2.5}$ mapping in 2010 [see Fig. 7(e)]. The $PM_{2.5}$ in YRD shows a spatial pattern of high in the northwest and low in the southeast in 2010, and high in the north and low in the south in 2020. From 2010 to 2020, the overall concentration shows a decreasing trend in the time series.

We projected the pixel-level $PM_{2.5}$ scenario to the year 2030 using SLM expressed in (9) based on the projected 2030 land coverage indices [see Fig. 8(a)]. The 2030 $PM_{2.5}$ scenario in YRD shows high concentrations in the northeast and low in the southeast. Among the 26 cities, Shanghai has the highest average of about 39.1 $\mu g/m^3$, followed by Nantong, Suzhou, and Yangzhou in Jiangsu Province, while Tāizhou in Zhejiang Province has the lowest average of about 26.2 $\mu g/m^3$ [see Fig. 8(b)]. Compared with 2010 and 2020, there are similarities in the overall distribution, with high $PM_{2.5}$ concentration in the north and low concentration in the south. Also, the average $PM_{2.5}$ have decreased in all subregions from 2010 to 2030, with the largest decrease of 47.3 $\mu g/m^3$ and the smallest decrease of 0.4 $\mu g/m^3$ at the pixel level [see Fig. 8(c)]. The large decreases are primarily found in the northwest (e.g., Tongling of Anhui about -38 $\mu g/m^3$), while the small decreases are mostly found in the east (e.g., Shanghai about -10.5 $\mu g/m^3$) and south (e.g., Zhoushan of Zhejiang about -11.9 $\mu g/m^3$). Fig. 8(d) shows that the largest rates of decline are about 50%–60%, occurring mostly in the northwest, while the smallest rates of decline are below 10%, occurring primarily in the east. This suggests significant regional heterogeneity in the rate of decline relative to 2010 as well.

The quantitative relations between land use and $PM_{2.5}$ were analyzed based on the proportion of each land-use type to the total land in each province and the average and standard deviation (STD) of $PM_{2.5}$ concentration in that province (see Table IV). The low $PM_{2.5}$ tends to be distributed in areas with a large proportion of forest, which is probably owing to the purifying effect of vegetation on $PM_{2.5}$ and the blocking effect of mountainous areas on $PM_{2.5}$ diffusion. While the high $PM_{2.5}$ tends to be distributed in areas with a high proportion of built-up and agricultural land, probably because high waste emissions from built-up lead to $PM_{2.5}$ emission, the agricultural located in the plains lead to $PM_{2.5}$ diffusion. In addition, the STD of $PM_{2.5}$ decreases in all four provinces during 2010–2030, indicating a reduction in intraprovince disparities of $PM_{2.5}$.

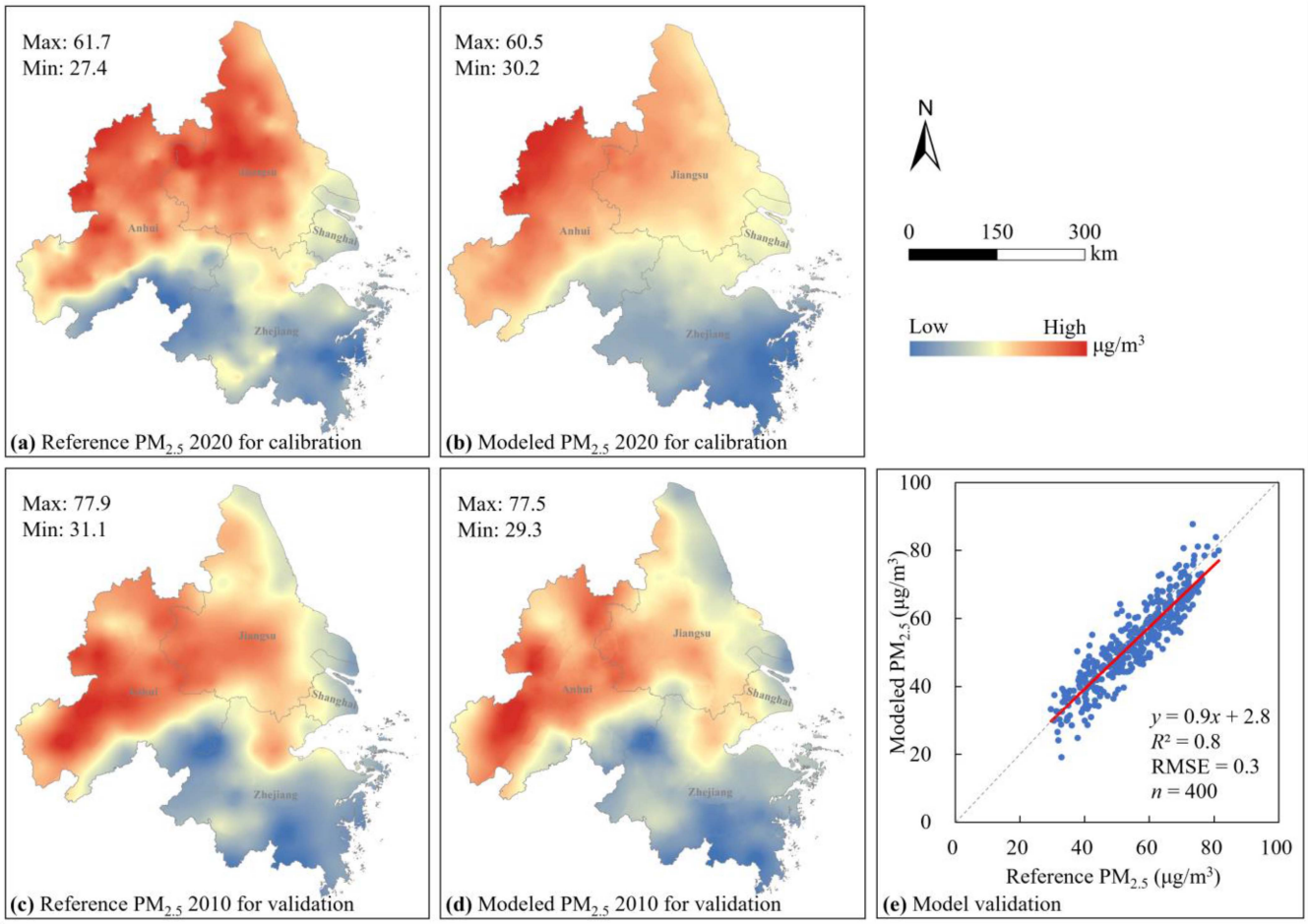

Fig. 7. Comparison of the reference and modeled $PM_{2.5}$ pattern in calibration and validation. (a) Reference $PM_{2.5}$ 2020 for calibration. (b) Modeled $PM_{2.5}$ 2020 for calibration. (c) Reference $PM_{2.5}$ 2010 for validation. (d) Modeled $PM_{2.5}$ 2010 for validation. (e) Model validation.

IV. Discussion

A. Three Crucial Aspects of the Methods

Based on the fact that $PM_{2.5}$ concentration is closely related to land use, and thus to land coverage indices, we projected the pixel-level $PM_{2.5}$ scenario by predicting land-use patterns, with a case study of YRD. Methodologically, the three crucial aspects of implementing pixel-level $PM_{2.5}$ scenario projection include land-use pattern projection, land coverage indices projection, and pixel-level $PM_{2.5}$ projection considering spatial dependence.

The land-use pattern projection depends not only on the simulation model but also on the thematic resolution of the land-use classification. Many models of land-use simulation, including SLEUTH, CLUE-S, CA-Markov, FLUS, and UrbanCA, have been well applied in China [34], [47]; however, for the prediction of land-use and $PM_{2.5}$ in YRD, we applied a new Futureland model that can apply different influencing factors to different land uses [29], thus achieving high-precision land-use simulation. As for land-use classification, we have considered four categories, including built-up, agricultural, forest, and water, where the built-up is primarily associated with the production and formation of $PM_{2.5}$, the agricultural is mostly related to the $PM_{2.5}$ diffusion, and forest and water are primarily correlated with its purification [48], which integrally contribute to its distribution. Probably, a finer thematic resolution is more favorable for $PM_{2.5}$ prediction, but it may lead to more complex land-use simulation and higher uncertainty in the future land scenario, and thus a more implausible $PM_{2.5}$ scenario. Therefore, our selection of land-use types and thematic resolution is a compromise of the simulation complexity and accuracy.

$PM_{2.5}$ is a continuously distributed entity across space, and achieving its pixel-level prediction requires identifying closely related other entities, and these are the land coverage indices. In this study, we selected indices, including NDBI, NDVI, and NDWI, according to the land-use pattern. Among these, NDBI depicts impervious surface coverage that reflects human activities that may result in the emission of $PM_{2.5}$ [49], NDVI depicts vegetation coverage that reflects the greenness, and NDWI depicts the water coverage and reflects the humidity associated with the ecosystem that affects the $PM_{2.5}$ purification [50]. The pixel-level scenario projection of $PM_{2.5}$ is attributed to the accurate prediction of land coverage indices, which can be retrieved from the future land-use scenario. In addition, SLVM was used to predict the land coverage indices, taking into account the structural variation in long time series and local variation in

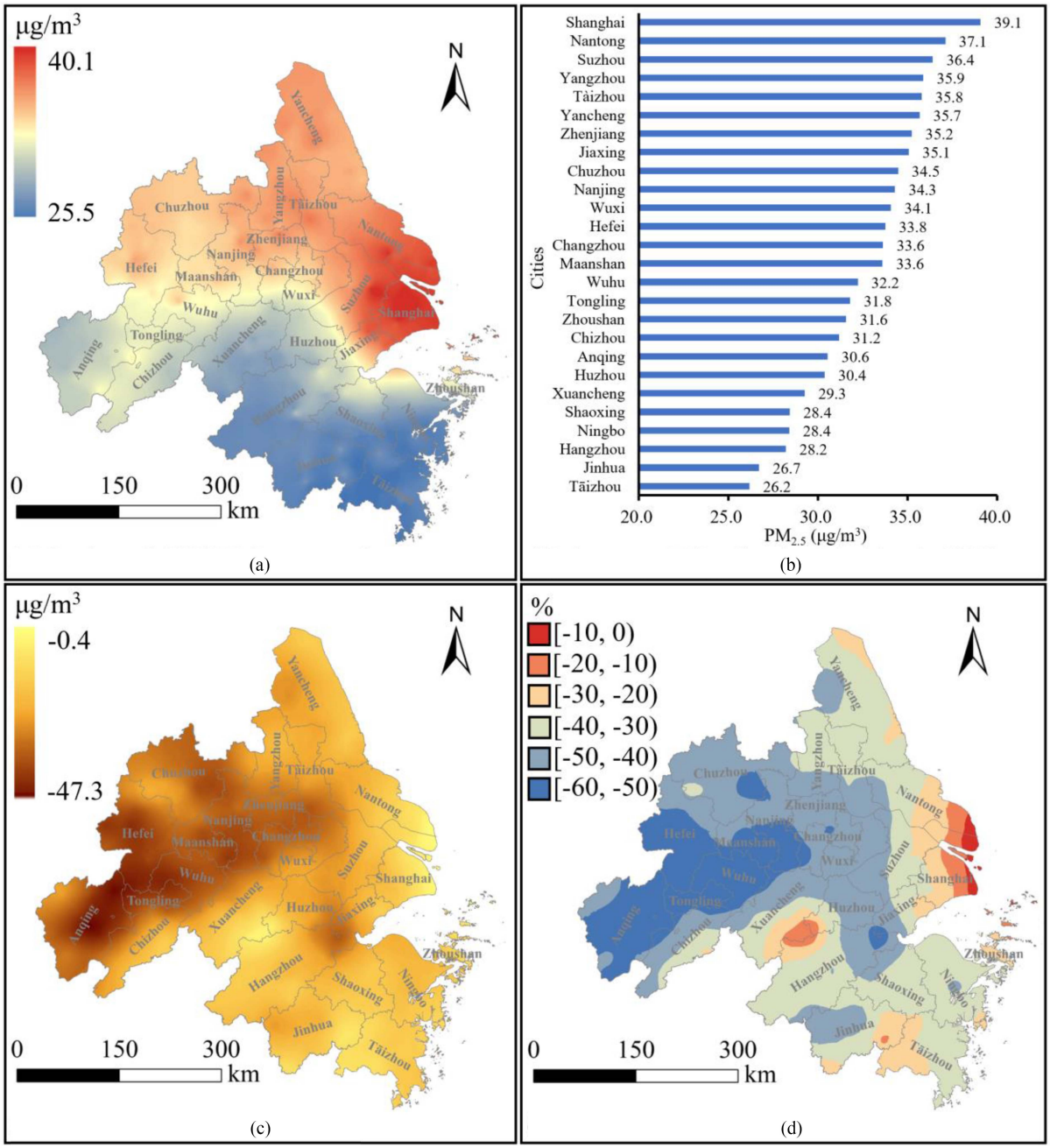

Fig. 8. Projected $PM_{2.5}$ scenario for the year 2030 and its change 2010–2030. (a) Projected 2030 $PM_{2.5}$ scenario. (b) Average $PM_{2.5}$ for the 26 cities in 2030. (c) $PM_{2.5}$ variation 2010–2030. (d) $PM_{2.5}$ growth rate 2010–2030.

land-use pattern. This approach has also been applied in earlier studies on pixel-level prediction of land surface temperatures [42], and it applies to scenario prediction for most continuously distributed entities.

$PM_{2.5}$ has significant spatial dependence effects because air pollution is prone to spread and migrate across space [51]. In addition, it has been recognized that the results may be biased if the spatial effect of $PM_{2.5}$ is ignored when analyzing its relationship with related variables [52], and this also occurs in the spatial prediction of $PM_{2.5}$. SLM is a spatial autoregressive model considering the spatial dependence effects of $PM_{2.5}$ by introducing the spatially weighted neighbors. Therefore, in connecting land coverage indices and $PM_{2.5}$, we have taken into account not only the land-use change but also the spatial dependence effects of $PM_{2.5}$, resulting in outcomes more in line with the knowledge and earlier findings of $PM_{2.5}$ distribution. We applied $PM_{2.5}$ data from ground monitoring stations in 2020 to calibrate the model and applied the historical gridded $PM_{2.5}$ [46] in 2010 to validate the method and outcomes. We used the 2020 data for model calibration because these ground monitoring stations have been releasing observations since 2013 and the earlier 2010 data for model validation because of the availability of the $PM_{2.5}$ product from Washington University. The product has been widely accepted because it is accurate by combining AOD,

TABLE IV
LAND-USE PROPORTION AND $PM_{2.5}$ OF THE FOUR PROVINCES 2010–2030

Land-use and $PM_{2.5}$			Administrative region			
			Shanghai	Jiangsu	Zhejiang	Anhui
2010	Land-use (%)	Built-up	37.2	10.9	7.8	5.0
		Agricultural	50.1	70.3	37.2	53.3
		Forest	0.8	3.2	51.7	34.4
		Water	11.9	15.6	3.3	7.3
		Total	100.0	100.0	100.0	100.0
	$PM_{2.5}$ ($\mu g/m^3$)	Average	49.5	59.4	45.0	62.4
		STD	4.8	6.1	7.0	9.6
2020	Land-use (%)	Built-up	42.5	18.0	12.8	7.1
		Agricultural	41.6	61.8	30.6	52.0
		Forest	3.2	3.6	51.4	33.8
		Water	12.7	16.6	5.2	7.1
		Total	100.0	100.0	100.0	100.0
	$PM_{2.5}$ ($\mu g/m^3$)	Average	41.6	51.8	38.3	48.4
		STD	1.5	4.1	4.5	7.0
2030	Land-use (%)	Built-up	46.2	21.3	16.8	10.7
		Agricultural	37.2	57.6	26.8	47.8
		Forest	3.5	4.0	50.8	33.6
		Water	13.1	17.1	5.6	7.9
		Total	100.0	100.0	100.0	100.0
	$PM_{2.5}$ ($\mu g/m^3$)	Average	39.1	35.6	28.4	32.0
		STD	0.5	1.5	2.6	2.0

chemical transport modeling, and ground-based measurements [46]. In addition, when projecting the $PM_{2.5}$ pattern for 2030, the model calibrated using $PM_{2.5}$ in 2020 and validated using $PM_{2.5}$ in 2010 is more accurate than the one calibrated using $PM_{2.5}$ in 2010 and validated using $PM_{2.5}$ in 2020.

B. *Impacts of $PM_{2.5}$ Pattern in YRD*

The results show significant decreases in past and future $PM_{2.5}$ in YRD, suggesting a leading position for the region in China's "peak emissions by 2030 and carbon neutrality by 2060" goal. Although the decrease might be influenced by many factors, the promotion of ecological civilization policies and the increase of environmental protection awareness should probably be considered as the dominants [53], [54]. China's official environmental protection authority (gov.cn) has reported a reduction in $PM_{2.5}$ and an increase in days of good air quality in YRD from 2020 to 2021. Also, a report of air quality assessment from Peking University indicates continued significant declines in $PM_{2.5}$ (research.pku.edu.cn). These bulletins and reports have confirmed our results that significant decreases in $PM_{2.5}$ have occurred and will also continue to occur in YRD. Despite the significant urban expansion in YRD over the years, the implementation of environmental protection policies and the use of new energy sources have managed to reduce $PM_{2.5}$, suggesting the possibility of the harmonious development of urbanization, industrialization, and the ecological environment.

Concerning the spatial profile, the reduction of $PM_{2.5}$ varies among provinces in YRD, leading to a west–east shift in the gravity center of $PM_{2.5}$ distribution. Our results show significant spatial heterogeneity in $PM_{2.5}$ of YRD, with high in the north and low in the south, which is primarily due to the agricultural and built-up in the north and forest in the south. Specifically, in 2030, $PM_{2.5}$ in Shanghai and Nantong, situated in the east of YRD, is about 39.1 $\mu g/m^3$ and 37.1 $\mu g/m^3$, ranking first and second, respectively. This may be largely due to the impact of high-intensity socioeconomic activities, high population density, and the impact of large-scale urban development and industrialization, leading to great pressure on environmental protection. In addition, given the significant spatial heterogeneity in $PM_{2.5}$,

the implementation of the overall optimization of the national territory (land use) spatial planning should be considered under the method of "integrated development of YRD." With the optimization of land allocation, it is recommended that measures, such as energy conservation and emission reduction, should also be implemented, and cross-regional transfer of $PM_{2.5}$ pollution as evidenced by the spatial dependence effects should be avoided to jointly create a "Green YRD" [55].

C. Comparison With Previous Studies

Concerning the $PM_{2.5}$ analysis based on remote sensing and GIS, quite a few publications have performed distribution estimation, spatiotemporal evolution analysis, and future prediction. $PM_{2.5}$ distribution estimation is usually performed using regression methods, including the land-use regression (LUR) model and GTWR model [56], [57]. LUR is constructed as a linear model of the relationship between $PM_{2.5}$ and different environmental features (i.e., land use, population density, road network, and meteorological conditions) [58], [59], whereas GTWR of $PM_{2.5}$ modeling is an improved model taking into account time and space [57]. In fact, the $PM_{2.5}$ concentration at one location is also influenced by the concentration in its surroundings; thus, we employed a spatial autoregressive model (i.e., SLM) to delineate the spatial dependence effects of $PM_{2.5}$ to achieve good modeling performance. In many case studies, the goodness-of-fit (i.e., R^2) of the modeling is around 0.69–0.82 [60], [61], [62], while the goodness-of-fit of our modeling is 0.87, confirming the superiority of our results. This suggests that our approach provides an applausive alternative for the estimation of the $PM_{2.5}$ distribution.

The spatiotemporal evolution of $PM_{2.5}$ was found correlated to land-use change; specifically in our study, $PM_{2.5}$ is positively correlated with built-up and negatively correlated with forests and water bodies. Underlying the above relationships as a modeling basis, our results indicate that $PM_{2.5}$ in YRD shows high values in the north and low values in the south and decreases over time, confirming the findings of previous studies [63]. We, therefore, confirm the following remarks that implementing energy-saving and emission-reduction policies, alleviating traffic on urban land, and increasing green space can help reduce air pollutants [64]. With the analysis of the spatiotemporal evolution of $PM_{2.5}$, its prediction allows us to better formulate the above policies, and the prediction can be carried out on a variety of scales, such as hourly [65], daily [66], weekly [24], and monthly [67]. These short-term $PM_{2.5}$ predictions are also helpful in alerting severe pollution incidents, which are crucial for human health improvement [68]. In our study, we predicted the pixel-level $PM_{2.5}$ scenarios over a long term (ten years) based on the future land-use scenario projected by Futureland. The long-term $PM_{2.5}$ prediction is a valuable attempt because it is important for the overall optimization of the national territory spatial planning.

V. Conclusion

We proposed a new method to project pixel-level $PM_{2.5}$ scenario over a long term and large scale by considering the land-use change and spatial dependence effects. In this method, we applied SLM to construct a relationship between land coverage indices and $PM_{2.5}$ concentration, where the impact of neighboring $PM_{2.5}$ was considered for the analysis. The future land-use scenario that was used to derive the future land coverage indices was performed using the Futureland model. Using this method, we then projected the spatial pattern of $PM_{2.5}$ in YRD in 2030 based on Landsat images, $PM_{2.5}$ data from ground monitoring stations, and historical gridded $PM_{2.5}$. The results reveal that the spatiotemporal dynamics of $PM_{2.5}$ are correlated with land-use changes, and specifically, $PM_{2.5}$ is positively correlated with built-up and negatively correlated with forest and water. This study also indicates that, from 2010 to 2030, $PM_{2.5}$ in YRD tends to decrease and shows high values in the north and low in the south. Our projections suggest that the ecological and economic integration of the region will contribute to sustainable development.

Pixel-level estimation and prediction of $PM_{2.5}$ are important issues in air pollution research and prevention, and our methods and case study show the efficiency for future projection of $PM_{2.5}$. Limitations of our study also exist, for example, we did not consider meteorological data and only predicted one scenario. Further work should consider the different projections of land use and $PM_{2.5}$ scenarios under different development pathways, such as the shared socioeconomic pathways. The spatial dependence effects of $PM_{2.5}$ are closely related to the spatial scale of data; thus, it is necessary to examine the influence of spatial weight definition and spatial scale on future scenario prediction in the future. Overall, the present method can be easily applied to predict pixel-level $PM_{2.5}$ patterns elsewhere, as well as to project the spatial pattern of other environmental parameters, such as ozone and sulfur dioxide.

References

[1] Y. Zhang, X. Chen, Y. Mao, C. Shuai, L. Jiao, and Y. Wu, "Analysis of resource allocation and $PM_{2.5}$ pollution control efficiency: Evidence from 112 Chinese cities," *Ecol. Indicators*, vol. 127, Aug. 2021, Art. no. 107705, doi: 10.1016/j.ecolind.2021.107705.

[2] M. R. Yaseen, Q. Ali, and M. T. I. Khan, "General dependencies and causality analysis of road traffic fatalities in OECD countries," *Environ. Sci. Pollut. Res.*, vol. 25, no. 20, pp. 19612–19627, Jul. 2018, doi: 10.1007/s11356-018-2146-4.

[3] S. Zheng, J. Wang, C. Sun, X. Zhang, and M. E. Kahn, "Air pollution lowers Chinese urbanites' expressed happiness on social media," *Nat. Hum. Behav.*, vol. 3, no. 3, pp. 237–243, Mar. 2019, doi: 10.1038/s41562-018-0521-2.

[4] C. Zhao et al., "Long-term exposure to $PM_{2.5}$ aggravates pulmonary fibrosis and acute lung injury by disrupting Nrf2-mediated antioxidant function," *Environ. Pollut.*, vol. 313, Nov. 2022, Art. no. 120017, doi: 10.1016/j.envpol.2022.120017.

[5] R. Burnett et al., "Global estimates of mortality associated with long-term exposure to outdoor fine particulate matter," *Proc. Nat. Acad. Sci.*, vol. 115, no. 38, pp. 9592–9597, Sep. 2018, doi: 10.1073/pnas.1803222115.

[6] M. A. Zoran, R. S. Savastru, D. M. Savastru, and M. N. Tautan, "Assessing the relationship between surface levels of $PM_{2.5}$ and PM_{10} particulate matter impact on COVID-19 in Milan, Italy," *Sci. Total Environ.*, vol. 738, Oct. 2020, Art. no. 139825, doi: 10.1016/j.scitotenv.2020.139825.

[7] M. Sorek-Hamer, R. Chatfield, and Y. Liu, "Review: Strategies for using satellite-based products in modeling $PM_{2.5}$ and short-term pollution episodes," *Environ. Int.*, vol. 144, Nov. 2020, Art. no. 106057, doi: 10.1016/j.envint.2020.106057.

[8] P. Maheshwarkar and R. Sunder Raman, "Population exposure across central India to $PM_{2.5}$ derived using remotely sensed products in a three-stage statistical model," *Sci. Rep.*, vol. 11, no. 1, Jan. 2021, Art. no. 544, doi: 10.1038/s41598-020-79229-7.

[9] Y. Chen, Y. Zhou, and X. Zhao, "$PM_{2.5}$ over North China based on MODIS AOD and effect of meteorological elements during 2003–2015," *Front. Environ. Sci. Eng.*, vol. 14, no. 2, 2020, Art. no. 23, doi: 10.1007/s11783-019-1202-8.

[10] Y. Sathe, S. Kulkarni, P. Gupta, A. Kaginalkar, S. Islam, and P. Gargava, "Application of moderate resolution imaging spectroradiometer (MODIS) aerosol optical depth (AOD) and weather research forecasting (WRF) model meteorological data for assessment of fine particulate matter ($PM_{2.5}$) over India," *Atmos. Pollut. Res.*, vol. 10, no. 2, pp. 418–434, Sep. 2018, doi: 10.1016/j.apr.2018.08.016.

[11] C. Lin et al., "Observation of $PM_{2.5}$ using a combination of satellite remote sensing and low-cost sensor network in Siberian urban areas with limited reference monitoring," *Atmos. Environ.*, vol. 227, Apr. 2020, Art. no. 117410, doi: 10.1016/j.atmosenv.2020.117410.

[12] P. Muthukumar et al., "Predicting $PM_{2.5}$ atmospheric air pollution using deep learning with meteorological data and ground-based observations and remote-sensing satellite big data," *Air Qual., Atmos., Health*, vol. 15, no. 7, pp. 1221–1234, Nov. 2022, doi: 10.1007/s11869-021-01126-3.

[13] N. Fann, E. Coffman, B. Timin, and J. T. Kelly, "The estimated change in the level and distribution of $PM_{2.5}$-attributable health impacts in the United States: 2005–2014," *Environ. Res.*, vol. 167, pp. 506–514, Nov. 2018, doi: 10.1016/j.envres.2018.08.018.

[14] W. J. Requia, B. A. Coull, and P. Koutrakis, "Evaluation of predictive capabilities of ordinary geostatistical interpolation, hybrid interpolation, and machine learning methods for estimating $PM_{2.5}$ constituents over space," *Environ. Res.*, vol. 175, pp. 421–433, Aug. 2019, doi: 10.1016/j.envres.2019.05.025.

[15] J. Ma, Y. Ding, J. C. P. Cheng, F. Jiang, and Z. Wan, "A temporal-spatial interpolation and extrapolation method based on geographic long short-term memory neural network for $PM_{2.5}$," *J. Cleaner Prod.*, vol. 237, Nov. 2019, Art. no. 117729, doi: 10.1016/j.jclepro.2019.117729.

[16] Y. Du, Q. Wan, H. Liu, Hao Liu, K. Kapsar, and J. Peng, "How does urbanization influence $PM_{2.5}$ concentrations? Perspective of spillover effect of multi-dimensional urbanization impact," *J. Cleaner Prod.*, vol. 220, pp. 974–983, 2019, doi: 10.1016/j.jclepro.2019.02.222.

[17] X. Mao, L. Wang, X. Pan, M. Zhang, X. Wu, and W. Zhang, "A study on the dynamic spatial spillover effect of urban form on $PM_{2.5}$ concentration at county scale in China," *Atmos. Res.*, vol. 269, May 2022, Art. no. 106046, doi: 10.1016/j.atmosres.2022.106046.

[18] Z. Su, L. Lin, Y. Chen, and H. Hu, "Understanding the distribution and drivers of $PM_{2.5}$ concentrations in the Yangtze River Delta from 2015 to 2020 using random forest regression," *Environ. Monit. Assessment*, vol. 194, no. 4, Mar. 2022, Art. no. 284, doi: 10.1007/s10661-022-09934-5.

[19] A. Mhawish et al., "Estimation of high-resolution $PM_{2.5}$ over the Indo-Gangetic plain by fusion of satellite data, meteorology, and land use variables," *Environ. Sci. Technol.*, vol. 54, no. 13, pp. 7891–7900, Jul. 2020, doi: 10.1021/acs.est.0c01769.

[20] Y. Shi, C. Ren, K. K.-L. Lau, and E. Ng, "Investigating the influence of urban land use and landscape pattern on $PM_{2.5}$ spatial variation using mobile monitoring and WUDAPT," *Landscape Urban Plan.*, vol. 189, pp. 15–26, Sep. 2019, doi: 10.1016/j.landurbplan.2019.04.004.

[21] D. A. Wood, "Trend decomposition aids forecasts of air particulate matter ($PM_{2.5}$) assisted by machine and deep learning without recourse to exogenous data," *Atmos. Pollut. Res.*, vol. 13, no. 3, Mar. 2022, Art. no. 101352, doi: 10.1016/j.apr.2022.101352.

[22] M. Z. Joharestani, C. Cao, X. Ni, B. Bashir, and S. Talebiesfandarani, "$PM_{2.5}$ prediction based on random forest, XGBoost, and deep learning using multisource remote sensing data," *Atmosphere*, vol. 10, no. 7, 2019, Art. no. 373, doi: 10.3390/atmos10070373.

[23] W. Zhou, X. Wu, S. Ding, X. Ji, and W. Pan, "Predictions and mitigation strategies of $PM_{2.5}$ concentration in the Yangtze River Delta of China based on a novel nonlinear seasonal grey model," *Environ. Pollut.*, vol. 276, May 2021, Art. no. 116614, doi: 10.1016/j.envpol.2021.116614.

[24] J. Bi, K. E. Knowland, C. A. Keller, and Y. Liu, "Combining machine learning and numerical simulation for high-resolution $PM_{2.5}$ concentration forecast," *Environ. Sci. Technol.*, vol. 56, no. 3, pp. 1544–1556, Feb. 2022, doi: 10.1021/acs.est.1c05578.

[25] N. Liu, B. Zou, S. Li, H. Zhang, and K. Qin, "Prediction of $PM_{2.5}$ concentrations at unsampled points using multiscale geographically and temporally weighted regression," *Environ. Pollut.*, vol. 284, Sep. 2021, Art. no. 117116, doi: 10.1016/j.envpol.2021.117116.

[26] J. Jiang, Z. Xu, J. Lu, and D. Sun, "Does network externality of urban agglomeration benefit urban economic growth—A case study of the Yangtze River Delta," *Land*, vol. 11, no. 4, 2022, Art. no. 586, doi: 10.3390/land11040586.

[27] Y. Feng et al., "The effects of factor generalization scales on the reproduction of dynamic urban growth," *Geo-Spatial Inf. Sci.*, vol. 25, no. 3, pp. 457–475, Jul. 2022, doi: 10.1080/10095020.2022.2025748.

[28] M. Kummu, M. Taka, and J. H. A. Guillaume, "Gridded global datasets for gross domestic product and human development index over 1990–2015," *Sci. Data*, vol. 5, Feb. 2018, Art. no. 180004, doi: 10.1038/sdata.2018.4.

[29] Y. Feng and F. Gao, "Futureland: The state-of-art software of complex land use change modeling and prediction," 2021. [Online]. Available: researchgate.net/publication/356978377

[30] C. A. Orieschnig, G. Belaud, J.-P. Venot, S. Massuel, and A. Ogilvie, "Input imagery, classifiers, and cloud computing: Insights from multi-temporal LULC mapping in the Cambodian Mekong Delta," *Eur. J. Remote Sens.*, vol. 54, no. 1, pp. 398–416, Jan. 2021, doi: 10.1080/22797254.2021.1948356.

[31] Y. Feng and Y. Liu, "A cellular automata model based on nonlinear kernel principal component analysis for urban growth simulation," *Environ. Plan. B, Plan. Des.*, vol. 40, no. 1, pp. 117–134, Feb. 2013, doi: 10.1068/b37142.

[32] Y. Feng and Y. Liu, "Scenario prediction of emerging coastal city using CA modeling under different environmental conditions: A case study of Lingang New City, China," *Environ. Monit. Assessment*, vol. 188, no. 9, Sep. 2016, Art. no. 540, doi: 10.1007/s10661-016-5558-y.

[33] I. Chowdhuri, S. C. Pal, and R. Chakrabortty, "Flood susceptibility mapping by ensemble evidential belief function and binomial logistic regression model on river basin of eastern India," *Adv. Space Res.*, vol. 65, no. 5, pp. 1466–1489, Mar. 2020, doi: 10.1016/j.asr.2019.12.003.

[34] Y. Feng and X. Tong, "A new cellular automata framework of urban growth modeling by incorporating statistical and heuristic methods," *Int. J. Geograph. Inf. Sci.*, vol. 34, no. 1, pp. 74–97, 2020, doi: 10.1080/13658816.2019.1648813.

[35] J. Liao et al., "A neighbor decay cellular automata approach for simulating urban expansion based on particle swarm intelligence," *Int. J. Geograph. Inf. Sci.*, vol. 28, no. 4, pp. 720–738, Jan. 2014, doi: 10.1080/13658816.2013.869820.

[36] P. Saha, R. Mitra, K. Chakraborty, and M. Roy, "Application of multi layer perceptron neural network Markov chain model for LULC change detection in the Sub-Himalayan North Bengal," *Remote Sens. Appl., Soc. Environ.*, vol. 26, Apr. 2022, Art. no. 100730, doi: 10.1016/j.rsase.2022.100730.

[37] M. Xi et al., "Development of a parallel computing-based Futureland model for multiple land-use simulation: A case study in Shanghai," *Geocarto Int.*, vol. 38, no. 1, Dec. 2023, Art. no. 2216675, doi: 10.1080/10106049.2023.2216675.

[38] Y. Zha, J. Gao, and S. Ni, "Use of normalized difference built-up index in automatically mapping urban areas from TM imagery," *Int. J. Remote Sens.*, vol. 24, no. 3, pp. 583–594, Feb. 2003, doi: 10.1080/01431160304987.

[39] N. Pettorelli, J. O. Vik, A. Mysterud, J.-M. Gaillard, C. J. Tucker, and N. C. Stenseth, "Using the satellite-derived NDVI to assess ecological responses to environmental change," *Trends Ecol. Evol.*, vol. 20, no. 9, pp. 503–510, Sep. 2005, doi: 10.1016/j.tree.2005.05.011.

[40] S. K. McFeeters, "The use of the normalized difference water index (NDWI) in the delineation of open water features," *Int. J. Remote Sens.*, vol. 17, no. 7, pp. 1425–1432, May 1996, doi: 10.1080/01431169608948714.

[41] Y. Zheng, L. Tang, and H. Wang, "An improved approach for monitoring urban built-up areas by combining NPP-VIIRS nighttime light, NDVI, NDWI, and NDBI," *J. Cleaner Prod.*, vol. 328, Dec. 2021, Art. no. 129488, doi: 10.1016/j.jclepro.2021.129488.

[42] Y. Feng, H. Li, X. Tong, L. Chen, and Y. Liu, "Projection of land surface temperature considering the effects of future land change in the Taihu Lake basin of China," *Glob. Planet. Change*, vol. 167, pp. 24–34, Aug. 2018, doi: 10.1016/j.gloplacha.2018.05.007.

[43] Z. Wu, Y. Chen, Y. Han, T. Ke, and Y. Liu, "Identifying the influencing factors controlling the spatial variation of heavy metals in suburban soil using spatial regression models," *Sci. Total Environ.*, vol. 717, May 2020, Art. no. 137212, doi: 10.1016/j.scitotenv.2020.137212.

[44] L. Anselin, "Under the hood issues in the specification and interpretation of spatial regression models," *Agricultural Econ.*, vol. 27, no. 3, pp. 247–267, 2002, doi: 10.1111/j.1574-0862.2002.tb00120.x.

[45] N. Kayet et al., "Spatiotemporal LULC change impacts on groundwater table in Jhargram, West Bengal, India," *Sustain. Water Resour. Manage.*, vol. 5, no. 3, pp. 1189–1200, 2019, doi: 10.1007/s40899-018-0294-9.
[46] A. van Donkelaar et al., "Monthly global estimates of fine particulate matter and their uncertainty," *Environ. Sci. Technol.*, vol. 55, no. 22, pp. 15287–15300, Nov. 2021, doi: 10.1021/acs.est.1c05309.
[47] H. Ma et al., "State of the art on artificial intelligence in land use simulation," *Complexity*, vol. 2022, pp. 1–19, 2022, doi: 10.1155/2022/2291508.
[48] Q. She et al., "Air quality and its response to satellite-derived urban form in the Yangtze River Delta, China," *Ecol. Indicators*, vol. 75, pp. 297–306, Apr. 2017, doi: 10.1016/j.ecolind.2016.12.045.
[49] Y. Zhu et al., "Quantifying spatiotemporal heterogeneities in $PM_{2.5}$-related health and associated determinants using geospatial big data: A case study in Beijing," *Remote Sens.*, vol. 14, no. 16, Aug. 2022, Art. no. 4012, doi: 10.3390/rs14164012.
[50] M. Meftahi, M. Monavari, M. Kheirkhah Zarkesh, A. Vafaeinejad, and A. Jozi, "Achieving sustainable development goals through the study of urban heat island changes and its effective factors using spatio-temporal techniques: The case study (Tehran City)," *Natural Resour. Forum*, vol. 46, no. 1, pp. 88–115, Feb. 2022, doi: 10.1111/1477-8947.12245.
[51] Q. Xie, X. Xu, and X. Liu, "Is there an EKC between economic growth and smog pollution in China? New evidence from semiparametric spatial autoregressive models," *J. Cleaner Prod.*, vol. 220, pp. 873–883, 2019, doi: 10.1016/j.jclepro.2019.02.166.
[52] V. J. Berrocal et al., "A comparison of statistical and machine learning methods for creating national daily maps of ambient $PM_{2.5}$ concentration," *Atmos. Environ.*, vol. 222, Feb. 2020, Art. no. 117130, doi: 10.1016/j.atmosenv.2019.117130.
[53] Y. Feng, M. Ning, Y. Lei, Y. Sun, W. Liu, and J. Wang, "Defending blue sky in China: Effectiveness of the 'air pollution prevention and control action plan' on air quality improvements from 2013 to 2017," *J. Environ. Manage.*, vol. 252, Dec. 2019, Art. no. 109603, doi: 10.1016/j.jenvman.2019.109603.
[54] L. Qu et al., "Evaluating the meteorological normalized $PM_{2.5}$ trend (2014–2019) in the '2+26' region of China using an ensemble learning technique," *Environ. Pollut.*, vol. 266, no. 3, Nov. 2020, Art. no. 115346, doi: 10.1016/j.envpol.2020.115346.
[55] T. Feng, H. Du, Z. Lin, and J. Zuo, "Spatial spillover effects of environmental regulations on air pollution: Evidence from urban agglomerations in China," *J. Environ. Manage.*, vol. 272, Oct. 2020, Art. no. 110998, doi: 10.1016/j.jenvman.2020.110998.
[56] G. Hoek et al., "A review of land-use regression models to assess spatial variation of outdoor air pollution," *Atmos. Environ.*, vol. 42, no. 33, pp. 7561–7578, Oct. 2008, doi: 10.1016/j.atmosenv.2008.05.057.
[57] Q. He and B. Huang, "Satellite-based high-resolution $PM_{2.5}$ estimation over the Beijing-Tianjin-Hebei region of China using an improved geographically and temporally weighted regression model," *Environ. Pollut.*, vol. 236, pp. 1027–1037, May 2018, doi: 10.1016/j.envpol.2018.01.053.
[58] K. de Hoogh et al., "Development of West-European $PM_{2.5}$ and NO_2 land use regression models incorporating satellite-derived and chemical transport modelling data," *Environ. Res.*, vol. 151, pp. 1–10, Nov. 2016, doi: 10.1016/j.envres.2016.07.005.
[59] Z. Li, K.-F. Ho, H.-C. Chuang, and S. H. L. Yim, "Development and intercity transferability of land-use regression models for predicting ambient PM_{10}, $PM_{2.5}$, NO_2 and O_3 concentrations in Northern Taiwan," *Atmos. Chem. Phys.*, vol. 21, no. 6, pp. 5063–5078, 2021, doi: 10.5194/acp-21-5063-2021.
[60] M. Brauer et al., "Estimating long-term average particulate air pollution concentrations: Application of traffic indicators and geographic information systems," *Epidemiology*, vol. 14, no. 2, pp. 228–239, Mar. 2003, doi: 10.1097/01.EDE.0000041910.49046.9B.
[61] D. K. Moore, M. Jerrett, W. J. Mack, and N. Kunzli, "A land use regression model for predicting ambient fine particulate matter across Los Angeles, CA," *J. Environ. Monit.*, vol. 9, no. 3, pp. 246–252, Mar. 2007, doi: 10.1039/b615795e.
[62] X. Fang, B. Zou, X. Liu, T. Sternberg, and L. Zhai, "Satellite-based ground $PM_{2.5}$ estimation using timely structure adaptive modeling," *Remote Sens. Environ.*, vol. 186, pp. 152–163, Dec. 2016, doi: 10.1016/j.rse.2016.08.027.
[63] D. Yang et al., "Predicting spatio-temporal concentrations of $PM_{2.5}$ using land use and meteorological data in Yangtze River Delta, China," *Stochastic Environ. Res. Risk Assessment*, vol. 32, pp. 2445–2456, 2018, doi: 10.1007/s00477-017-1497-6.
[64] D. Lu, W. Mao, D. Yang, J. Zhao, and J. Xu, "Effects of land use and landscape pattern on $PM_{2.5}$ in Yangtze River Delta, China," *Atmos. Pollut. Res.*, vol. 9, no. 4, pp. 705–713, Jul. 2018, doi: 10.1016/j.apr.2018.01.012.
[65] G. Huang, X. Li, B. Zhang, and J. Ren, "$PM_{2.5}$ concentration forecasting at surface monitoring sites using GRU neural network based on empirical mode decomposition," *Sci. Total Environ.*, vol. 768, May 2021, Art. no. 144516, doi: 10.1016/j.scitotenv.2020.144516.
[66] J. Zhu, F. Deng, J. Zhao, and H. Zheng, "Attention-based parallel networks (APNet) for $PM_{2.5}$ spatiotemporal prediction," *Sci. Total Environ.*, vol. 769, May 2021, Art. no. 145082, doi: 10.1016/j.scitotenv.2021.145082.
[67] Z. He, Q. Guo, Z. Wang, and X. Li, "Prediction of monthly $PM_{2.5}$ concentration in Liaocheng in China employing artificial neural network," *Atmosphere*, vol. 13, no. 8, Aug. 2022, Art. no. 1221, doi: 10.3390/atmos13081221.
[68] W. Mao, W. Wang, L. Jiao, S. Zhao, and A. Liu, "Modeling air quality prediction using a deep learning approach: Method optimization and evaluation," *Sustain. Cities Soc.*, vol. 65, Feb. 2021, Art. no. 102567, doi: 10.1016/j.scs.2020.102567.

Panli Tang received the M.S. degree in geography from the Wuhan University of Technology, Wuhan, China, in 2022. She is currently working toward the Ph.D. degree in geomatics with Tongji University, Shanghai, China.

Yongjiu Feng received the Ph.D. degree in geomatics from Tongji University, Shanghai, China, in 2009.

He is currently a Professor and an Associate Dean of the College of Surveying and Geo-Informatics, Tongji University. His research interests include spatial modeling, synthetic aperture radar, and radar detection of the moon and deep space.

Xiaohua Tong (Senior Member, IEEE) received the Ph.D. degree in traffic engineering from Tongji University, Shanghai, China, in 1999.

He is currently a Professor with the College of Surveying and Geo-Informatics, Tongji University. His research interests include photogrammetry and remote sensing, trust in spatial data, and image processing for high-resolution satellite images.

Mengrong Xi is currently working toward the Ph.D. degree in geomatics with Tongji University, Shanghai, China.

Pengshuo Li received the B.E. degree in geomatics engineering in 2021 from Tongji University, Shanghai, China, where he is currently working toward the M.S. degree in surveying and mapping science and technology.

Shurui Chen received the M.S. degree in marine sciences from Shanghai Ocean University, Shanghai, China, in 2021. He is currently working toward the Ph.D. degree in geomatics with Tongji University, Shanghai, China.

Rong Wang received the M.S. degree in marine sciences from Shanghai Ocean University, Shanghai, China, in 2022. She is currently working toward the Ph.D. degree in artificial intelligence with Tongji University, Shanghai, China.

Xiong Xu (Member, IEEE) received the Ph.D. degree in photogrammetry and remote sensing from Wuhan University, Wuhan, China, in 2013.

He is currently an Associate Professor with the College of Surveying and Geoinformatics, Tongji University, Shanghai, China. His current research interests include multi- and hyperspectral image processing, deep learning in remote sensing, and remote sensing applications.

Chao Wang received the Ph.D. degree in cartography and geography information system from East China Normal University, Shanghai, China, in 2016.

He is currently an Associate Professor with Tongji University, Shanghai, China. His research interests include hyperspectral remote sensing, and planetary atmosphere.

Peng Chen received the Ph.D. degree in geomatics from Tongji University, Shanghai, China, in 2006.

He is currently an Associate Professor with the College of Surveying and Geoinformatics, Tongji University, Shanghai, China. His research interests include spatial analysis and high-speed video measurement.